ARTICLE

Resistive Switching in Single Epitaxial ZnO Nanoislands

Jing Qi,[†,‡,‖,*] Mario Olmedo,[‡,‖] Jingjian Ren,[‡] Ning Zhan,[‡] Jianze Zhao,[‡,§] Jian-Guo Zheng,[⊥] and Jianlin Liu[‡,*]

[†]The Key Laboratory for Magnetism and Magnetic Materials of MOE, Lanzhou University, Lanzhou 730000, China, [‡]Quantum Structures Laboratory, Department of Electrical Engineering, University of California, Riverside, California 92521, United States, [§]School of Physics and Optoelectronic Engineering, Dalian University of Technology, Dalian 116024, China, and [⊥]The Laboratory for Electron and X-ray Instrumentation, California Institute for Telecommunication and Information Technology (Calit2), University of California, Irvine, California 92697, United States. [‖]These authors contributed equally to this work.

ABSTRACT

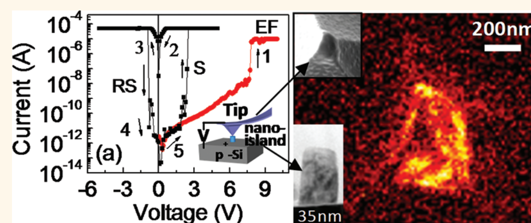

Resistive memory is one of the most promising candidates for next-generation nonvolatile memory technology due to its variety of advantages, such as simple structure and low-power consumption. Bipolar resistive switching behavior was observed in epitaxial ZnO nanoislands with base diameters and heights ranging around 30 and 40 nm, respectively. All four different states (initial, electroformed, ON, and OFF) of the nanoscale resistive memories were measured by conductive atomic force microscopy immediately after the voltage sweeping was performed. Auger electron spectroscopy and other experiments were also carried out to investigate the switching mechanism. The formation and rupture of conducting filaments induced by oxygen vacancy migration are responsible for the resistive switching behaviors of ZnO resistive memories at the nanoscale.

KEYWORDS: resistive memory scaling · switching mechanism · C-AFM · ZnO · nanoisland · conducting filament

Resistive random access memory (RRAM) has been attracting attention for high-density, high-speed, and low-power nonvolatile memory technology owing to its simple structure, high-density integration, low-power consumption, fast operation, and strong potential for fabricating multilevel-per-cell memories.[1−5] RRAM based on various oxides including NiO,[6−11] TiO_2,[12−16] CuO,[17] CoO,[18,19] ZnO,[20−22] and others[2,23−25] have been widely investigated. Among numerous theoretical models proposed for explaining the resistive switching behavior, the formation/rupture of filaments consisting of oxygen vacancies or metallic ions in the insulating matrix was believed to be responsible for the resistance switching of both macroscopic and microscopic oxide RRAM devices.[2,6,7,9,10,13−19,23,24] However, the microscopic details of the ion migration during electroforming, SET, and RESET processes still need to be clarified, especially for the conducting filaments consisting of oxygen vacancies. Furthermore, whether this model is applicable for resistive switching in nanoscale devices with sizes on the order of several to several tenths of nanometers remains unclear.

While it is important to study the switching mechanism for understanding the scalability of RRAM, it is crucial to reliably fabricate and characterize RRAM cells with a size beyond the limitation of state-of-the-art lithography length scale. Toward scaling down the size of the memory devices, the bottom-up self-assembly of nanowires emerges as a popular method.[11,12,26] For example, Nagashima *et al.*[26] demonstrated multistate resistive switching memory effect in a single cobalt oxide nanowire. However, the memory window for a nanowire device is usually less than 10^3. In addition, the switching voltages are also very high. These results are partly due to the fact that the distance between the two electrodes is usually larger than 100 nm. In order to achieve a large memory window and low switching voltage, it is necessary to keep the distance between the two electrodes (top and bottom contacts in metal/insulator/metal structure case) to be less than 50 nm. In this paper, ZnO single-crystal nanoislands with base diameters of 20−60 nm and heights of about 40 nm, which have suitable structure for improving memory performance and understanding the mechanism at the nanoscale, were self-assembled on silicon substrates. Conductive atomic force microscopy (C-AFM) was used to study these nanoislands, virtually forming nanoscale devices with a small distance between the top electrode (C-AFM tip) and the bottom electrode (substrate), which is the height of

* Address correspondence to qijing@lzu.edu.cn, jianlin@ee.ucr.edu.

Received for review July 14, 2011 and accepted January 18, 2012.

Published online January 18, 2012
10.1021/nn204809a

© 2012 American Chemical Society

nano the nanoislands. Bipolar resistive memory effect with memory windows on the order of 10^7 for a single ZnO nanoisland is demonstrated. The mechanism of the switching behavior and the ion migration during switching processes in the nanoscale resistive memories are discussed in detail.

RESULTS AND DISCUSSION

Self-assembled ZnO single-crystal nanoislands were grown on Si(100) substrates by plasma-assisted molecular beam epitaxy (MBE). The details of growth can be found in the Supporting Information. These nanoislands were then characterized using scanning electron microscopy (SEM) and transmission electron microscopy (TEM) techniques. Figures 1 shows (a) top-view, (b) cross-sectional SEM images, (c) diameter, and (d) height distributions of the ZnO nanoislands. The diameters of these ZnO nanoislands are between 10 and 60 nm, while the heights are between 20 and 70 nm. The density of the nanoislands is about 100/μm^2. Figure 1e is a bright-field TEM micrograph of the nanoislands. The selected area electron diffraction (SAED) pattern (Figure 1f) from the area displayed in Figure 1e includes diffraction spots from both the Si substrate and ZnO nanoislands. The spots from Si form a network, and six of the spots close to the transmission beam (center of the pattern) are marked with lines. Additional spots result from ZnO nanoislands, which is confirmed by dark-field imaging of the spot marked in a circle in Figure 1f. The result is shown in the inset of Figure 1e. The fact that the nanoisland is lit up in the inset means the existence of the correlation between the circled spot and the crystal. The scattered diffraction spots suggest that the ZnO nanoislands are in single-crystalline form. Moreover, the interplanar spacings can be determined from the distances between these additional spots and the transmission beam. As marked in Figure 1f, the measured interplanar spacings are consistent with those of ZnO. The orientation relationship between the additional spots and Si-related spots shows that the ZnO crystals are randomly oriented. High-resolution TEM (HRTEM) image shown in Figure 1g for one ZnO nanoisland provides further evidence that the nanoislands are ZnO single crystals. The inset of Figure 1g is a fast Fourier transform (FFT) of the image. The interplanar spacings measured from the image and FFT are consistent with those of ZnO in the zone axis of [$\bar{1}2\bar{1}0$]. AFM was also carried out to confirm the morphology of the ZnO nanoislands (Supporting Information).

Typical current–voltage (I–V) results for the ZnO nanoscale resistive memories are shown in Figure 2a. An electroforming process is necessary, which occurred at a voltage of approximately +8 V under a current compliance of 10 μA during the first applied external voltage sweeping from 0 to 10 V, as shown in

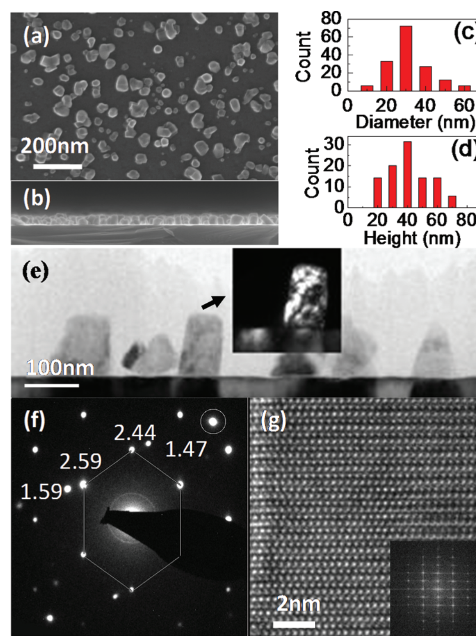

Figure 1. (a) Top-view, (b) cross-sectional SEM images, (c) diameter, and (d) height distributions of ZnO nanoislands. (e) Bright-field TEM micrograph of the nanoislands. (f) SAED pattern from the area displayed in (e) including diffraction spots from both the Si substrate and ZnO nanoislands. (g) HRTEM image from one ZnO nanoisland. Inset in (e): dark-field image recorded with the spot marked in a circle in (f). Inset in (g): fast Fourier transform (FFT) of the image (g).

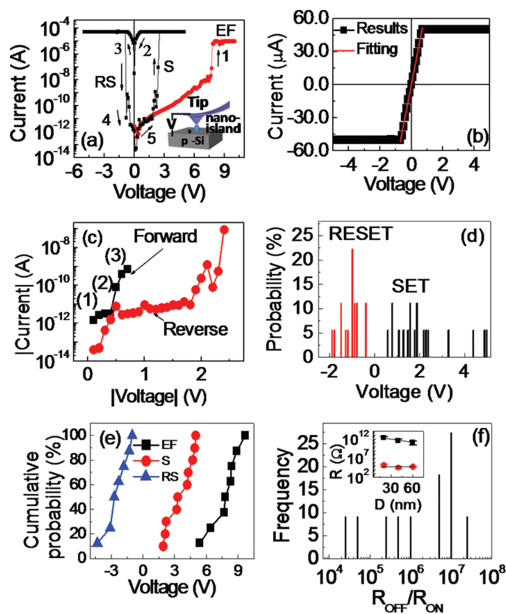

Figure 2. (a) Typical I–V characteristics of a ZnO nanoisland resistive memory. Inset: schematic illustration of the experiment setup for switching a ZnO nanoisland with a C-AFM tip. (b) Linear fitting for the I–V curve of the LRS. (c) I–V curve in semilogarithmic scale for the HRS. (d) Typical V_{SET} (black) and V_{RESET} (red) distributions of different cycles for one nanoscale resistive memory. (e) Distributions of electroforming (EF), SET (S), and RESET (RS) voltages for different ZnO nanoisland resistive memories. (f) Histogram of R_{OFF}/R_{ON} for different nanoscale resistive memories. Inset: relationship between resistance and diameter of the ZnO nanoislands for both ON- and OFF-states.

the red circle line denoted as process 1. The presence of a forming process is one of the unique features of the filament model.[26] After the forming process, the bipolar resistive switching $I-V$ curve, conducted by an application of voltage cycles ((2) +5 V → 0 V; (3) 0 V → −5 V; (4) −5 V → 0 V; (5) 0 V → +5 V), demonstrates high degree of repeatability at both the same (Figure 2a) and different current compliance (Figure S3a). The behavior of bipolar switching at different current compliance provides the potential application of ZnO nanoisland resistive memory in multilevel-per-cell memory.[26] The ZnO nanoisland resistive memory is kept in low resistive state (LRS or ON-state) during voltage sweeping of processes 2 and 3. During process 4, a pronounced change of resistance from LRS to high resistive state (HRS or OFF-state) was observed at −0.8 V, which is defined as the "RESET" process, and corresponding voltage as RESET voltage (V_{RESET}). Subsequently, an opposite "SET" process with SET voltage (V_{SET}) can be observed as the voltage swept reversely from 0 to 5 V (process 5), evidenced by a two-step switching from HRS to LRS. The first switching occurred between 1.8 and 2.0 V. The second one took place at 2.3−2.5 V after the resistance of the nanoscale resistive memory stayed at an intermediate state from 2.0 to 2.3 V. This kind of two-step SET process was even more obvious at higher current compliance, as shown in Figure S3a, which implies another way of multilevel data storage as long as an effective control over threshold voltage could be realized.[27] A similar two-step SET process was also observed by Kim *et al.* in TiO_2 systems,[28] in which filamentary switching *via* partial rupture and recovery of the ruptured portion of filaments were used to explain the two-step SET process.

The memory window defined by the two resistance states

$$(R_{OFF} - R_{ON})/R_{ON} \sim R_{OFF}/R_{ON} \tag{1}$$

is more than 10^6 over a large range of reading voltage (−0.4 V ∼ −0.1 V and +0.1 V ∼ +1.7 V) from Figure 2a. The large memory window would allow a periphery circuit to very easily distinguish the information stored in the ON- and OFF-state. It is also beneficial for fabricating multilevel memory by using different current compliance.

Figure 2b shows that the ON-state $I-V$ curve can be well fitted with linear fitting, in which the reverse of the slope, about 10^4 Ω, is the resistance of the ON-state resistive memory. This linear $I-V$ relationship clearly exhibits an ohmic conduction behavior, which is caused by the formation of conductive metallic filaments in the ZnO nanoisland during the SET process. Similar result was reported by Yang *et al.* in a RRAM device based on ZnO:Mn thin film.[27] In the meantime, the $I-V$ curve is similar to that of a practical diode for the OFF-state (HRS), as shown in Figure 2c. The Si substrate here serves as the p-type material in the heterojunction diode system, which is composed of a C-AFM tip, n-type ZnO nanoisland, and p^+-Si substrate. ZnO serves as the n-type material in which oxygen vacancy should be the intrinsic donor of the electron carrier because ZnO nanoislands were deposited in a zinc-rich condition. Under negative bias, the system is a forward biased diode. The conduction mechanism is dominated by three kinds of current as shown in Figure 2c: (1) recombination−generation current; (2) the diffusion current; and (3) the diffusion current at high-level injection. The $I-V$ curve can be described by

$$I = I_s(\exp(qV/nkT) - 1) \tag{2}$$

where I, I_s, V, kT, q, and n are the junction current, saturation current, applied voltage, thermal energy, magnitude of electronic charge, and the fitting factor for different dominated current mechanism, respectively.[29] When positive bias is applied, the system is a reverse biased diode. Reverse leakage current is due to generation−recombination and surface effects. The junction breakdown is corresponding to the SET process, which forms the filamentary conducting paths.[25]

Figure 2d shows distributions of SET and RESET voltages (V_{RESET} and V_{SET}) for different sweeping cycles performed on a single ZnO nanoisland resistive memory, in which, if a two-step SET or RESET process happened, the voltage for the first one was utilized for statistics. V_{RESET} and V_{SET} distribute in the ranges of −0.4 to −1.9 V and 0.6 to 5.0 V, respectively. V_{SET} distribution shows much more scattering than that of V_{RESET}, which is another piece of evidence that conducting filaments play a crucial role in bipolar resistive switching characteristics in ZnO nanoscale resistive memories. According to the conducting filament model,[27,30] during filament formation and rupture process, the formation of a filament (SET) should be more random than the destruction of an existing filament (RESET) because the formation process is determined by the competition among different filamentary paths. Therefore, larger variations in V_{SET} than in V_{RESET} should be expected, which is also validated in other oxide systems.[31,32]

The $I-V$ measurements depicted previously were conducted on dozens of similar nanoislands. A new C-AFM tip was used for every single nanoscale resistive memory measurement to avoid effects caused by the change of the tip happening during $I-V$ characterization. During these measurements, similar $I-V$ characteristics as shown in Figure 2a were obtained. Figure 2e,f shows distributions of electroforming, SET, RESET voltages, and memory window R_{OFF}/R_{ON} for these measured ZnO nanoisland resistive memories, respectively. Data for V_{SET}, V_{RESET}, and R_{OFF}/R_{ON} are those of the first voltage sweeping loop after electroforming. The electroforming voltage (V_{EF}) distributes between 5.4 and 9.7 V, while V_{SET} and V_{RESET} are in the range of +1.9 ∼ +5 V and −1 ∼ −4.3 V, respectively, according to cumulative probability results shown in Figure 2e. These voltage ranges are reasonable because

the crystal orientation, oxygen vacancy density, diameter, and thickness of the measured ZnO single-crystal nanoislands are slightly different from one to another. From the results of R_{OFF}/R_{ON} frequency for different measured nanoscale resistive memories, as shown in Figure 2f, the memory windows are no less than 10^6 for over 70% ZnO nanoscale resistive memories. Resistance ratios between OFF- and ON-state are several orders larger than reported ones based on undoped ZnO materials with sizes of square micrometers.[33] The nanoisland size effect on RRAM switching behavior was also studied. All nanoislands between 20 and 60 nm have similar switching behavior, while the R ratio increases with the decrease of the nanoisland size from 60 to 20 nm, as shown in the inset of Figure 2f. There is no obvious relationship between the ON-state resistance and size of nanoislands. However, OFF-state resistance decreases slightly with the increase of the nanoisland size, similar to the reported results of RRAM at microscale.[34]

To clarify the operation mechanism of the nanoscale resistive memories, current distribution of a single nanoisland at the four different states was mapped using C-AFM. Figure 3 shows a typical topographic image of a ZnO nanoisland resistive memory (Figure 3a) and its C-AFM images, showing local current distributions for different states of initial (Figure 3b), electroformed (Figure 3c), OFF (Figure 3d), and ON (Figure 3e,f), which were measured immediately after switching. During electroforming, SET, and RESET processes, which were completed by sweeping applied voltage (processes 1−5), the conducting tip was fixed in the center of the ZnO nanoisland (the circle positions of the images in Figure 3). In addition, all C-AFM images were obtained with a bias of −2.0 V applied to the tip, which did not change the initial state of the measured nanoislands as evidenced by the substantial number of measurements. In the initial state, current is almost evenly distributed in the whole area of the nanoisland, at a level of about 20 pA, as shown in Figure 3b. This current is attributed to oxygen vacancies, which act as donors in ZnO materials.[35] The existence of oxygen vacancies was proven by a deep level peak of around 2.5 eV in the photoluminescence (PL) spectrum[36] and metallic Zn peak at 992.0 eV in high spatial resolution Auger electron spectroscopy (HSR-AES)[37] shown in Figure S3. After electroforming (Figure 3c), the current with the highest value of 40 pA is mainly distributed around the edge area of the nanoisland, while the center area is highly resistive. In order to ensure that the bias of −2 V during the C-AFM measurement will not RESET the nanoisland from ON-state to OFF-state, the current compliance was increased from 50 to 500 μA, which elevates the RESET voltage to as high as −4 V, as shown in Figure S3a. From Figure 3d, it is obvious that the whole nanoisland was switched to OFF-state after the RESET process. After the SET process, the nanoisland was switched back to ON-state, as shown in Figure 3e. These results show that the size of the actual

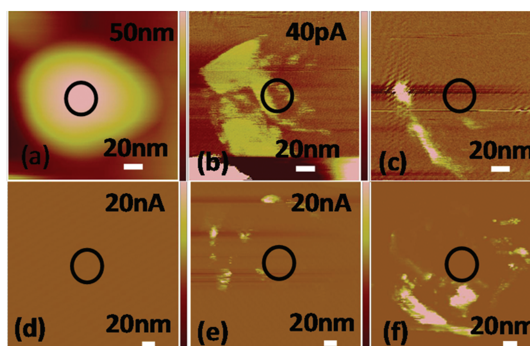

Figure 3. (a) AFM height image recorded in air on a ZnO nanoisland on a Si substrate for the initial state. (b−f) Local current distributions of a nanoscale resistive memory for four different states: (b) initial, (c) electroformed, (d) OFF, and (e,f) two ON-states.

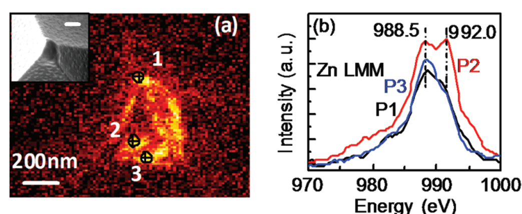

Figure 4. (a) AES Zn map of a C-AFM tip after electrical measurement. Inset: top-view SEM image of this tip. (b) HSR-AES high-energy resolution spectra of Zn LMM from the three spots with diameters of 10 nm marked in (a) for this C-AFM tip.

working memory cell depends on the size of the nanoisland in the ZnO nanoisland resistive memory case. The ZnO nanoisland was switched between ON- and OFF-states several times. The C-AFM images were also recorded each time, and Figure 3f shows another ON-state image. Comparing these images, such as Figure 3e,f, it was noticed that every time the nanoisland was switched to the ON-state, the position of the higher current spots changed, which proves that, during the SET process, there is competition among different filament paths, as evidenced by the distribution trait of V_{SET} and V_{RESET} in Figure 2d. It can also be obtained from C-AFM images of ON-states that the size of high current spots can be smaller than 5 nm, which shows the potential of scaling down the device to 5 nm.

An interesting phenomenon that occurred after electrical measurements was a noticeable change in nanoisland height and base diameter as a result of the obvious change of the AFM image size of the nanoislands, as shown in Figure S3f, implying that some material had been transferred to the tip during $I-V$ characterization. Figure 4a shows the AES Zn map of a C-AFM tip after electrical characterization. The inset is the corresponding top-view SEM image of the tip. Three points with diameters of 10 nm marked in Figure 4a were chosen for HSR-AES high-energy resolution spectrum measurements to determine the chemical state of Zn in the coated layer. The results are shown in Figure 4b as P1, P2, and P3, respectively.

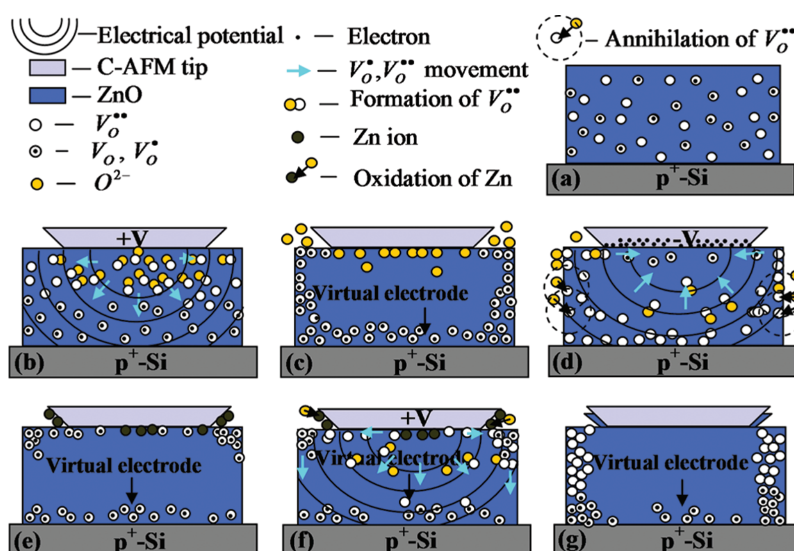

Figure 5. Schematic illustration of the resistive switching mechanism of the ZnO nanoisland resistive memory: (a) homogeneously conductive initial state, (b) electroforming process for oxygen vacancy generation and filament formation by movement of oxygen ions or oxygen vacancies, (c) electroformed state, (d) RESET process for oxygen vacancy annihilation and filament rupture by moving oxygen ions to V_O, (e) OFF-state, (f) SET process, and (g) ON-state.

A broad peak at 988.5 eV is dominant for point 1 and point 3, which can be ascribed to ZnO.[38] For point 2, another peak at 992.0 eV can also be observed, which is corresponding to the transition energy for Zn in the elemental form.[37] Additional SEM and energy-dispersive X-ray spectroscopy (EDX) measurements were carried out on these C-AFM tips and overused tips. Details can be found in the Supporting Information. These results indicate that Zn exists as both oxide and metal in the coated layer on the C-AFM tips after electrical measurements, which indicates that the conducting filaments consist of oxygen vacancies.

Finally, we discuss redox-controlled oxygen vacancy filament formation and rupture process, which are responsible for the bipolar resistive switching behavior in the C-AFM tip/ZnO nanoisland/p^+-Si resistive memory system (Figure 5). For initial state as shown in Figure 5a, oxygen vacancies are homogeneously distributed in the whole nanoisland and act as donors in ZnO materials,[35] leading to evenly distributed current, as shown in the C-AFM image of Figure 3b. Oxygen vacancies in ZnO should occur in three different charge states: V_O, $V_O^{\bullet}$, and $V_O^{\bullet\bullet}$.[39] V_O has captured two electrons and is electrically neutral relative to the lattice. $V_O^{\bullet}$ has trapped one electron and is positively charged, while $V_O^{\bullet\bullet}$ does not capture any electron and is doubly positively charged. During the electroforming process, as shown in Figure 5b, oxygen vacancies around the anode (C-AFM tip) lose the captured electrons and become positively charged, and then they move toward the cathode (substrate) and accumulate there, becoming a virtual cathode. At the same time, an oxidation reaction would happen around the anode according to[40,41]

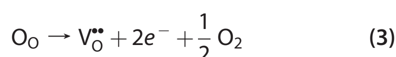

$$O_O \rightarrow V_O^{\bullet\bullet} + 2e^- + \frac{1}{2}O_2 \quad (3)$$

where O_O denotes oxygen ions on regular lattice sites. These $V_O^{\bullet\bullet}$ will also begin to move toward the virtual cathode, while interstitial oxygen ions are drawn to the anode and result in the production of oxygen gas there. The main routes for the oxygen movement and consequently oxygen vacancy movement should be along the surface and the edge of the nanoisland because oxygen grain boundary diffusion is 3−4 orders of magnitude greater than oxygen volume diffusion in ZnO.[41] Finally, oxygen vacancy conductive filaments are created along the edge of the nanoisland, as schematically viewed in Figure 5c, which is the completion of the electroforming process indicated by a sudden increase of current in the $I-V$ characterization (Figure 2a). The formation of oxygen vacancy filaments is proven by the current distribution in the C-AFM image result, as shown in Figure 3c, and the accumulation of ZnO and Zn metal on the tip, which indicates the reaction of redox, as shown in Figure 4. After electroforming, when the external voltage sweeps back to a less negative bias than V_{RESET}, V_O is electron-occupied and becomes electrically neutral. Due to electron shielding effect,[42] neutral V_O cannot capture charged interstitial O^{2-} effectively. When the bias voltage reaches V_{RESET} and is kept at V_{RESET} or a more negative value than V_{RESET} for enough time, as shown in Figure 2a, V_O loses its captured electrons and becomes $V_O^{\bullet\bullet}$, causing a significant increase of capturing probability of $V_O^{\bullet\bullet}$ to O^{2-},[42] as schematically shown in Figure 5d. The recombination between $V_O^{\bullet\bullet}$ and O^{2-} easily occurs near the edge of the nanoisland, where oxygen ions are supplied from the ambient. This recombination is corresponding to absorption of oxygen reported in other publications.[43] Finally, the filaments of oxygen vacancy are ruptured, as schematically shown in Figure 5e, during the RESET process, which is

indicated by the sudden decrease of the current (Figure 2a). At the same time, oxidation reaction in eq 3 keeps happening so that oxygen vacancies are continuously supplied. During the RESET process, many oxygen vacancies are dragged to the C-AFM tip. This causes the Zn ions around the tip to leave the ZnO lattice and transfer onto the surface of the tip as a result of the external electric field. These metal ions stay there as a metallic layer after getting electrons from the negative biased tip, which can be proven by the result shown in Figure 4b. After the RESET process, as shown in Figure 5f, when voltage sweeps back to a positive bias, oxygen vacancies are continuously created by the oxidation of the lattice oxygen ions, which is corresponding to desorption of oxygen.[43] All oxygen vacancies are then pushed away by the electric field from the tip mainly along the surface and edge of the nanoisland and gather there to restore the filaments or create new ones and switch the resistive memory to ON-state (Figure 5g). Meanwhile, oxygen ions are drawn back to the surface of the ZnO nanoisland near the tip where they recombine with some Zn ions that are pushed back from the tip by the electric field. During this SET process, some of the Zn ions on the surface of the tip are also oxidized. As a result, a mixture layer of ZnO and Zn metal is left on the surface of the C-AFM tip. If the $I-V$ characterization is performed for enough times by one tip, all Zn metals on the tip should be oxidized, as shown in Figure S4f. This picture of creation and rupture process of redox-controlled oxygen vacancy filaments can also be inferred from the morphology change of the nanoisland as shown in Figure S3c. According to Figure 3 and Figure 5, it can be concluded that grain edge plays a very important role in the formation and rupture of the conducting filaments consisting of oxygen vacancies in ZnO nanoscale resistive memories with cell diameters of 20−60 nm. This conclusion means that oxygen vacancy is a surface-related defect, as reviewed by Djurisic and Leung.[44]

CONCLUSIONS

Large memory window resistive switching behavior was observed in ZnO nanoisland resistive memories. Redox-controlled conducting filament formation/rupture consisting of oxygen vacancies, which is regarded as a possible mechanism for resistive memories at the macroscopic scale, was proven through various electrical and imaging results to also be responsible for the switching behavior of the ZnO nanoisland resistive memory with a dimension of as small as 20 nm. Furthermore, C-AFM results have revealed that the conducting filaments are formed on the edges of ZnO nanoisland and can have a size on the order of 5 nm, suggesting that ZnO-based RRAM is a promising technology for future nonvolatile memory at the scaled technology.

METHODS

Self-assembled ZnO single-crystal nanoislands were grown on precleaned p^+-Si(100) substrates at 350 °C in a radio frequency plasma-assisted MBE system. Electrical characterization utilizes an Agilent 4155C semiconductor parameter analyzer to apply sweeping voltages and obtain $I-V$ characteristics. For the C-AFM measurements, a Veeco Dimension Icon AFM with C-AFM capabilities is used. Both measurement systems are connected to the tip through a manual 3-way switch so that they can be easily switched without interference with each other during measurements, as shown in Figure S2. The tip is Co/Cr coated. The radius of curvature of the C-AFM tip apex is 20−50 nm. The typical diameter of contact area between the tip and a ZnO nanoisland during $I-V$ characterization is less than 20 nm, while during C-AFM mapping, it is about 5.2 nm, estimated using the DMT model.[45−47] $I-V$ characterization for state switching was done when the tip, acting as top contact of the nanoscale resistive memory cell, was fixed in the center of ZnO nanoisland with the Si substrate grounded, as shown in the inset of Figure 2a. The C-AFM images were measured immediately after state switching to obtain current distributions for four states (initial, electroformed, ON, and OFF) of the ZnO nanoisland resistive memory. SEM, EDX, HSR-AES, and AES elemental maps were utilized to study the layer coated on the C-AFM tips during the $I-V$ characterizations. The cross-sectional TEM specimens were prepared using FEI Quanta 3D FEG dual-beam focus ion beam instrument at UCI (Calit2 microscopy center). The original sample surface was protected by a carbon layer and an electron-beam-induced Pt layer. Bright-field and dark-field TEM images as well as selected area electron diffraction patterns were obtained using FEI CM-20 TEM operated at 200 kV with a LaB6 filament. The high-resolution TEM images were taken in a FEI Titan TEM operated at 300 kV with an image Cs corrector.

Conflict of Interest: The authors declare no competing financial interest.

Acknowledgment. The authors acknowledge the financial and program support of the Microelectronics Advanced Research Corporation (MARCO) and its Focus Center on Function Engineered Nano Architectonics (FENA), the DARPA/Defense Microeletctronics Activity (DMEA) under agreement number H94003-10-2-1003 (3D Electronics), and National Natural Science Foundation of China (No. 50902065). The authors also acknowledge Dennis Paul of Physical Electronics for AES and elemental map measurements using PHI 700Xi Scanning Auger Nanoprobe system. We thank Applied Technology Training Center at San Bernardino Community College District for letting us use the AFM equipment. Authors acknowledge the use of FEI Quanta 3D FEG dual-beam instrument and CM-20 TEM in Calit2Microscopy Center and Materials Characterization Center at Calit2, UCI. Authors also thank S.J. Xie for her assistance in HRTEM.

Supporting Information Available: The ZnO single-crystal nanoisland deposition detail, Figures S1−S6 with their main results briefly discussed. This material is available free of charge *via* the Internet at http://pubs.acs.org.

REFERENCES AND NOTES

1. Asamitsu, A.; Tomioka, Y.; Kuwahara, H.; Tokura, Y. Current Switching of Resistive States in Magnetoresistive Manganites. *Nature* **1997**, *388*, 50–52.
2. Waser, R.; Aono, M. Nanoionics-Based Resistive Switching Memories. *Nat. Mater.* **2007**, *6*, 833–840.
3. Lee, M. J.; Park, Y.; Suh, D. S.; Lee, E. H.; Seo, S.; Kim, D. C.; Jung, R.; Kang, B. S.; Ahn, S. E.; Lee, C. B.; *et al.* Two Series

Oxide Resistors Applicable to High Speed and High Density Nonvolatile Memory. *Adv. Mater.* **2007**, *19*, 3919–3923.
4. Son, J. Y.; Shin, Y. H.; Park, C. S. Bistable Resistive States of Amorphous $SrRuO_3$ Thin Films. *Appl. Phys. Lett.* **2008**, *92*, 133510.
5. Moreno, C.; Munuera, C.; Valencia, S.; Kronast, F.; Obradors, X.; Ocal, C. Reversible Resistive Switching and Multilevel Recording in $La_{0.7}Sr_{0.3}MnO_3$ Thin Films for Low Cost Nonvolatile Memories. *Nano Lett.* **2010**, *10*, 3828–3835.
6. Lee, M. J.; Han, S.; Jeon, S. H.; Park, B. H.; Kang, B. S.; Ahn, S. E.; Kim, K. H.; Lee, C. B.; Kim, C. J.; Yoo, I. K.; *et al.* Electrical Manipulation of Nanofilaments in Transition-Metal Oxides for Resistance-Based Memory. *Nano Lett.* **2009**, *9*, 1476–1481.
7. Ahn, S. H.; Lee, M. J.; Park, Y.; Kang, B. S.; Lee, C. B.; Kim, K. H.; Seo, S.; Suh, D. S.; Kim, D. C.; Hur, J.; *et al.* Write Current Reduction in Transition Metal Oxide Based Resistance Change Memory. *Adv. Mater.* **2008**, *20*, 924–928.
8. Yoshida, C.; Kinoshita, K.; Yamasaki, T.; Sugiyama, Y. Direct Observation of Oxygen Movement during Resistance Switching in NiO/Pt Film. *Appl. Phys. Lett.* **2008**, *93*, 042106.
9. Choi, J. S.; Kim, J. S.; Hwang, I. R.; Hong, S. H.; Jeon, S. H.; Kang, S. O.; Park, B. H.; Kim, D. C.; Lee, M. J.; Seo, S. Different Resistance Switching Behaviors of NiO Thin Films Deposited on Pt and $SrRuO_3$ Electrodes. *Appl. Phys. Lett.* **2009**, *95*, 022109.
10. Chang, S. H.; Lee, J. S.; Chae, S. C.; Lee, S. B.; Liu, C.; Kahng, B.; Kim, D. W.; Noh, T. W. Occurrence of Both Unipolar Memory and Threshold Resistance Switching in a NiO Film. *Phys. Rev. Lett.* **2009**, *102*, 026801.
11. Oka, K.; Yanagida, T.; Nagashima, K.; Tanaka, H.; Kawai, T. Nonvolatile Bipolar Resistive Memory Switching in Single Crystalline NiO Heterostructured Nanowires. *J. Am. Chem. Soc.* **2009**, *131*, 3434–3435.
12. Kim, S. I.; Lee, J. H.; Chang, Y. W.; Hwang, S. S.; Yoo, K. H. Reversible Resistive Switching Behaviors in NiO Nanowires. *Appl. Phys. Lett.* **2008**, *93*, 033503.
13. Kim, K. M.; Hwang, C. S. The Conical Shape Filament Growth Model in Unipolar Resistance Switching of TiO_2 Thin Film. *Appl. Phys. Lett.* **2009**, *94*, 122109.
14. Rohde, C.; Choi, B. J.; Jeong, D. S.; Choi, S.; Zhao, J. S.; Hwang, C. S. Identification of a Determining Parameter for Resistive Switching of TiO_2 Thin Films. *Appl. Phys. Lett.* **2005**, *86*, 262907.
15. Strukov, D. B.; Snider, G. S.; Stewart, D. R.; Williams, R. S. The Missing Memristor Found. *Nature* **2008**, *453*, 80–83.
16. Yang, J. J.; Pickett, M. D.; Li, X.; Ohlberg, D. A. A.; Stewart, D. R.; Williams, R. S. Memristive Switching Mechanism for Metal/Oxide/Metal Nanodevices. *Nat. Nanotechnol.* **2008**, *3*, 429–433.
17. Fujiwara, K.; Nemoto, T.; Rozenberg, M. J.; Nakamura, Y.; Takagi, H. Resistance Switching and Formation of a Conductive Bridge in Metal/Binary Oxide/Metal Structure for Memory Devices. *Jpn. J. Appl. Phys.* **2008**, *47*, 6266–6271.
18. Shima, H.; Takano, F.; Muramatsu, H.; Akinaga, H.; Tamai, Y.; Inque, I. H.; Takagi, H. Voltage Polarity Dependent Low-Power and High-Speed Resistance Switching in CoO Resistance Random Access Memory with Ta Electrode. *Appl. Phys. Lett.* **2008**, *93*, 113504.
19. Shima, H.; Takano, F.; Tamai, Y.; Akinaga, H.; Inoue, I. H. Synthesis and Characterization of Pt/Co−O/Pt Trilayer Exhibiting Large Reproducible Resistance Switching. *Jpn. J. Appl. Phys.* **2007**, *46*, L57–L60.
20. Kim, S.; Moon, H.; Gupta, D.; Yoo, S.; Choi, Y. Resistive Switching Characteristics of Sol−Gel Zinc Oxide Films for Flexible Memory Applications. *IEEE Trans. Electron Devices* **2009**, *56*, 696–699.
21. Xu, N.; Liu, L.; Sun, X.; Liu, X.; Han, D.; Wang, Y.; Han, R.; Kang, J.; Yu, B. Characteristics and Mechanism of Conduction/Set Process in TiN/ZnO/Pt Resistance Switching Random-Access Memories. *Appl. Phys. Lett.* **2008**, *92*, 232112.
22. Tseng, Z.; Kao, P.; Shih, M.; Huang, H.; Wang, J.; Chu, S. Electrical Bistability in Hybrid ZnO Nanorod/Polymethylmethacrylate Heterostructures. *Appl. Phys. Lett.* **2010**, *97*, 212103.
23. Nagashima, K.; Yanagida, T.; Oka, K.; Kawai, T. Unipolar Resistive Switching Characteristics of Room Temperature Grown SnO_2 Thin Films. *Appl. Phys. Lett.* **2009**, *94*, 242902.
24. Szot, K.; Speier, W.; Bihlmayer, G.; Waser, R. Switching the Electrical Resistance of Individual Dislocations in Single-Crystalline $SrTiO_3$. *Nat. Mater.* **2006**, *5*, 312–320.
25. Sawa, A. Resistive Switching in Transition Metal Oxides. *Mater. Today* **2008**, *11*, 28–36.
26. Nagashima, K.; Yanagida, T.; Oka, K.; Taniguchi, M.; Kawai, T.; Kim, J.; Park, B. H. Resistive Switching Multistate Nonvolatile Memory Effects in a Single Cobalt Oxide Nanowire. *Nano Lett.* **2010**, *10*, 1359–1363.
27. Yang, Y.; Pan, F.; Liu, Q.; Liu, M.; Zeng, F. Fully Room-Temperature-Fabricated Nonvolatile Resistive Memory for Ultrafast and High-Density Memory Application. *Nano Lett.* **2009**, *9*, 1636–1643.
28. Kim, K. M.; Choi, B. J.; Hwang, C. S. Localized Switching Mechanism in Resistive Switching of Atomic-Layer-Deposited TiO_2 Thin Films. *Appl. Phys. Lett.* **2007**, *90*, 242906.
29. Moll, J. L. The Evolution of the Theory of the Current Voltage Characteristics of p−n Junctions. *Proc. IRE* **1958**, *46*, 1076–1082.
30. Szot, K.; Speier, W.; Carius, R.; Zastrow, U.; Beyer, W. Localized Metallic Conductivity and Self-Healing during Thermal Reduction of $SrTiO_3$. *Phys. Rev. Lett.* **2002**, *88*, 075508.
31. Wang, Z.; Griffin, P. B.; McVittie, J.; Wong, S.; McIntyre, P. C.; Nishi, Y. Resistive Switching Mechanism in $Zn_xCd_{1-x}S$ Nonvolatile Memory Devices. *IEEE Electron Device Lett.* **2007**, *28*, 14–16.
32. Choi, B. J.; Jeong, D. S.; Kim, S. K.; Rohde, C.; Choi, S.; Oh, J. H.; Kim, H. J.; Hwang, C. S.; Szot, K.; Waser, R.; Reichenberg, B.; Tiedke, S. Resistive Switching Mechanism of TiO_2 Thin Films Grown by Atomic-Layer Deposition. *J. Appl. Phys.* **2005**, *98*, 033715.
33. Chang, W.; Lai, Y.; Wu, T.; Wang, S.; Chen, F.; Tsai, M. Unipolar Resistive Switching Characteristics of ZnO Thin Films for Nonvolatile Memory Applications. *Appl. Phys. Lett.* **2008**, *92*, 022110.
34. Wang, Y.; Liu, Q.; Long, S.; Wang, W.; Wang, Q.; Zhang, M.; Zhang, S.; Li, Y.; Zuo, Q.; Yang, J.; Liu, M. Investigation of Resistive Switching in Cu-Doped HfO_2 Thin Film for Multilevel Nonvolatile Memory Applications. *Nanotechnology* **2010**, *21*, 045202-1–045202-6.
35. Kasai, P. Electron Spin Resonance Studies of Donors and Acceptors in ZnO. *Phys. Rev.* **1963**, *130*, 989–995.
36. Vanheusden, K.; Seager, C. H.; Warren, W. L.; Tallant, D. R.; Voigt, J. A. Correlation between Photoluminescence and Oxygen Vacancies in ZnO Phosphors. *Appl. Phys. Lett.* **1996**, *68*, 403–405.
37. Panwar, B. S.; Bhattacharyya; Nagpal, A. B.; K., C.; Mall, R. P. Growth and Characterization of ZnO Films Deposited on a Monolithic Si_3N_4-SiO_2-Si Configuration. *Thin Solid Films* **1989**, *168*, 291–305.
38. Ren, F.; Jiang, C. Z.; Xiao, X. H. Fabrication of Single-Crystal ZnO film by Zn Ion Implantation and Subsequent Annealing. *Nanotechnology* **2007**, *18*, 285609.
39. Vanheusden, K.; Warren, W. L.; Seager, C. H.; Tallant, D. R.; Voigt, J. A. Mechanisms behind Green Photoluminescence in ZnO Phosphor Powders. *J. Appl. Phys.* **1996**, *79*, 7983–7990.
40. Merkle, R.; Maier, J. How Is Oxygen Incorporated into Oxides? A Comprehensive Kinetic Study of a Simple Solid-State Reaction with $SrTiO_3$ as a Model Material. *Angew. Chem., Int. Ed.* **2008**, *47*, 3874–3894.
41. Waser, R.; Dittmann, R.; Staikov, G.; Szot, K. Redox-Based Resistive Switching Memories—Nanoionic Mechanisms, Prospects, and Challenges. *Adv. Mater.* **2009**, *21*, 2632–2663.
42. Xu, N.; Gao, B.; Liu, L. F.; Sun, B.; Liu, X. Y.; Han, R. Q.; Kang, J. F.; Yu, B. A Unified Physical Model of Switching Behavior in Oxide-Based RRAM. *Symp. VLSI Tech.* **2008**, 100–101.
43. Soci, C.; Zhang, A.; Xiang, B.; Dayeh, S. A.; Aplin, D. P. R; Park, J.; Bao, X. Y.; Lo, Y. H.; Wang, D.; ZnO Nanowire, U. V.

Photodetectors with High Internal Gain. *Nano Lett.* **2007**, *7*, 1003.
44. Djurisic, A. B.; Leung, Y. H. Optical Properties of ZnO Nanostructures. *Small* **2006**, *2*, 944–961.
45. Derjaguin, B. V.; Muller, V. M.; Toporov, Y. P. Effect of Contact Deformations on the Adhesion of Particles. *J. Colloid Interface Sci.* **1975**, *53*, 314.
46. Muller, V. M.; Yushchenko, V. S.; Derjaguin, B. V. On the Influence of Molecular Forces on the Deformation of an Elastic Sphere and Its Sticking to a Rigid Plane. *J. Colloid Interface Sci.* **1980**, *77*, 91.
47. Muller, V. M.; Derjaguin, B. V.; Toporov, Y. P. On Two Methods of Calculation of the Force of Sticking of an Elastic Sphere to a Rigid Plane. *Colloids Surf.* **1983**, *7*, 251.